

# Hydrodynamic Inverse Faraday Effect in Two Dimensional Electron Liquid

S. O. Potashin,<sup>1</sup> V. Yu. Kachorovskii,<sup>1,2,3</sup> and M. S. Shur<sup>2</sup>

<sup>1</sup>*Ioffe Institute, 194021 St. Petersburg, Russia*

<sup>2</sup>*Rensselaer Polytechnic Institute, 12180, Troy, NY, USA*

<sup>3</sup>*CENTERA Laboratories, Institute of High Pressure Physics,  
Polish Academy of Sciences, 01-142 Warsaw, Poland*

We show that a small conducting object, such as a nanosphere or a nanoring, embedded into or placed in the vicinity of the two-dimensional electron liquid (2DEL) and subjected to a circularly polarized electromagnetic radiation induces “twisted” plasmonic oscillations in the adjacent 2DEL. The oscillations are rectified due to the hydrodynamic nonlinearities leading to the helicity sensitive circular dc current and to a magnetic moment. This hydrodynamic inverse Faraday effect (HIFE) can be observed at room temperature in different materials. The HIFE is dramatically enhanced in a periodic array of the nanospheres forming a resonant plasmonic coupler. Such a coupler exposed to a circularly polarized wave converts the entire 2DEL into a vortex state. Hence, the twisted plasmonic modes support resonant plasmonic-enhanced gate-tunable optical magnetization. Due to the interference of the plasmonic and Drude contributions, the resonances have an asymmetric Fano-like shape. These resonances present a signature of the 2DEL properties not affected by contacts and interconnects and, therefore, providing the most accurate information about the 2DEL properties. In particular, the widths of the resonances encode direct information about the momentum relaxation time and viscosity of the 2DEL.

## I. INTRODUCTION

Generation of stationary magnetic moment by a circularly polarized radiation is commonly referred to as the inverse Faraday effect (IFE) predicted by Pitaevskii [1] and first observed by van der Ziel et al. [2]. Although this effect is usually studied in magnetic materials [3–5], it can be also observed in conventional semiconductor nanostructures such as quantum dots and nanorings [6–15]. In particular, it was recently predicted [14, 15] that a circularly polarized radiation with the electric component  $\mathbf{E} = \mathbf{E}_\omega \exp(-i\omega t) + c.c.$  can excite a circular dc current in a nanoring, which, in turn, generates a magnetic moment

$$\mathbf{M} \propto i \mathbf{E}_\omega \times \mathbf{E}_\omega^*. \quad (1)$$

The proportionality coefficient in Eq. (1) is an odd function of frequency, so that the effect is sensitive to the helicity of polarization. Remarkably, IFE is dramatically enhanced in vicinity of plasmonic resonances [15]. Specifically, adjusting the plasmonic frequency in the nanoring to match the frequency of impinging radiation results in much larger optically-induced stationary magnetic field (up to 0.1 Gauss for typical parameters of a nanoring, see discussion in Ref. [15]). Hence, an array of nearly identical quantum rings should give rise to large optically-controlled macroscopic magnetization. This opens a wide avenue for applications in tunable optoelectronics, in particular, in the terahertz (THz) range of frequencies.

The key feature of the plasmonic-enhanced IFE as compared to other plasma wave related effects is the absence of the symmetry limitations for conversion of incoming radiation into a dc signal. Indeed, in conventional plasmonic devices such conversion requires an asymmetry of the system that determines direction of the dc current. In the two-dimensional structures, the asymmetry

can be created by the boundary conditions [16] or induced by ratchet effect (see Ref. 17 for review). The latter implies a special type of grating-gate couplers that could provide the required asymmetry. By contrast, IFE exists in fully symmetric rings [14, 15], and direction of the arising dc current is simply determined by the sign of the circular polarization. What is also important in view of possible applications for the THz plasmonics, the optically-induced dc current remains finite even in the longwavelength limit, when  $\mathbf{E}_\omega$  does not vary within the dimension of ring. Hence, the quantum nanorings and ring-based arrays can be used as an effective helicity-driven sensors for THz radiation [see estimates and discussion in Ref. [15]].

In this paper, we discuss the possibility of observing similar effects in 2D systems. We consider the excitation of circular plasmonic modes (“twisted plasmons”) and circular dc currents in two dimensional electronic liquid (2DEL). These modes are excited by a circularly polarized electromagnetic radiation impinging on the metallic or semiconducting nanosphere or nanoring embedded into or placed above the 2DEL and inducing rotating dipoles in these nanostructures (see Fig. 1a). Rectification of the twisted plasmons due to hydrodynamic nonlinearities leads to a helicity-sensitive circular DC current, and consequently, to a magnetic moment, thus demonstrating the hydrodynamic inverse Faraday effect (HIFE). If the nanospheres form a 2D crystal (see Fig. 1b), only the plasmons with the wave vectors forming inverse crystal lattice are excited, so that excitation spectrum becomes discrete. When the radiation frequency is close to any of the discrete plasmonic frequencies, the entire high-mobility 2DEL experiences a resonant circular plasmonic excitation. The rectification of these oscillations leads to plasmonic-enhanced DC current which oscillates in space. The circular dc current and magnetic

moment generated by this current show sharp HIFE resonances. Since the plasma wave frequency is tunable by the gate voltage and by an external magnetic field such a system can be used for the optical tunable magnetization of 2D systems. The typical 2DEL twisted plasmon frequencies are in the THz range, and this coupling system could be used for tunable THz electronic components, including frequency multipliers, modulators, absorbers, and mixers. Another key application is in the contactless characterization and parameter extraction of the 2DEL.

Apart from these applications, there are some very interesting fundamental aspects of the HIFE related to hydrodynamic approach in plasmonics, the field which explores how electromagnetic fields can be confined over dimensions much smaller than the radiation wavelength [18–24]. The hydrodynamic approach to the description of the electronic systems and, in particular, the plasma wave excitation, has a long history which can be traced back to the early work by Gurzhi [25] and by Jong and Molenkamp [26], where hydrodynamic effects on the electron and phonon transport were discussed and to the work by Dyakonov and Shur [16], which exploited the analogy between the “shallow water” hydrodynamics and that of the electron liquid in the two-dimensional (2D) gated systems. Many other beautiful hydrodynamic phenomena such as choking of electron flow [27], nonlinear rectification of the plasma waves [28, 29] and the formation of the plasmonic shock waves [30] have been subsequently proposed. Possible applications of these phe-

nomena to the plasma-wave electronics were intensively discussed (see reviews [31, 32]). More recent interest to the hydrodynamic phenomena in low-dimensional transport and plasmonics is driven by the emergence of the high-mobility nanostructures [33–41] and graphene [42–52] where the electron-electron collision-dominated transport regime can be reached.

Two issues that have been most actively discussed in recent years are the emergence of hydrodynamic regimes with nonzero vorticity (and their manifestation in the transport properties of the 2DEL) (see [40, 48–52] and references therein), as well as possible methods for measuring the electron viscosity by using dynamic excitations of 2DEL [40], and by nonlocal resistance measurements [48–52].

Here, we demonstrate that the electron flow with nonzero vorticity can be excited by circular polarized radiation. Importantly, we find that such states appear even in an ideal 2DEL with zero viscosity. We also find that the main effect of viscosity is broadening of the plasmonic resonances in the structure shown in Fig. 1b. Corresponding contribution to the resonance width is proportional to the kinematic viscosity and depends on the single geometrical factor—the distance  $d$  between nanospheres. This enables optical measurements of the electron liquid viscosity.

## II. MODEL

### A. Basic equations

In this work, we consider circular (twisted) plasmon excitation through the periodic array of metal objects (or semiconducting objects with high conductivity), such as nanospheres or nanorings, embedded into or placed in the vicinity of the 2DEL by using insulating matrix transparent for the THz radiation. To begin with, we consider the excitation by a single nanosphere (see Fig. 1 a), and then generalize the results in the case of the grating plasmonic coupler consisting of the a periodic array of nanospheres (see Fig. 1 b).

Circularly polarized electromagnetic radiation induces a rotating dipole potential in the nanosphere. As a result, an inhomogeneous field is formed, which, in turn, acts on the 2DEL. We will find the dc response of the system. We assume that: (i) electron-electron collisions prevail over scattering by phonons and impurities; (ii) the radiation wavelength is much larger than the radius of the nanosphere, so that the electric field of radiation is uniform; (iii) the system is gated. First assumption allows us to use the hydrodynamic approximation.

The 2D electron liquid is described by the hydrodynamic equations for the dimensionless electron concen-

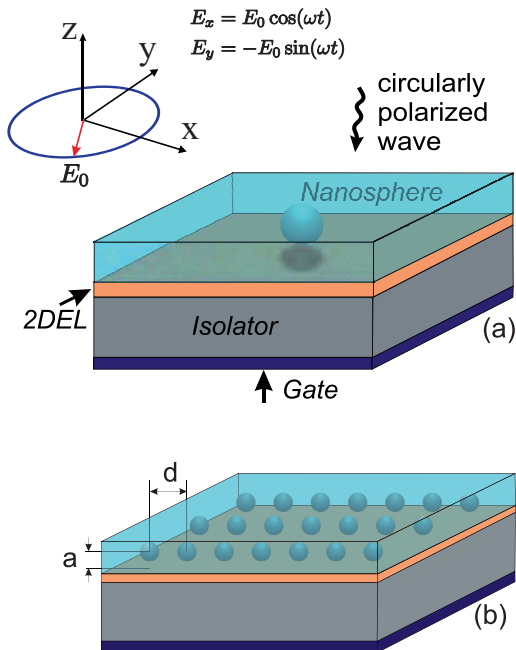


FIG. 1. Excitation of twisted plasmons in 2D electron liquid by a single nanosphere embedded into dielectric matrix and excited by circularly polarized radiation (a) or by an array of nanospheres forming plasmonic coupler (b)

tration  $n = (N - N_0)/N_0$  and velocity  $\mathbf{v}$ :

$$\frac{\partial n}{\partial t} + \text{div} [(1 + n)\mathbf{v}] = 0, \quad (2)$$

$$\frac{\partial \mathbf{v}}{\partial t} + (\mathbf{v}\nabla)\mathbf{v} + \gamma\mathbf{v} + s^2\nabla n - \nu\Delta\mathbf{v} = \frac{e\mathbf{E}}{m}. \quad (3)$$

Here  $N_0$  is equilibrium concentration,  $s$  is the plasma wave velocity,  $\gamma$  is the rate of the momentum relaxation,  $\omega$  is the radiation frequency,  $m$  is the electron mass, and  $\nu$  is the kinematic viscosity. The field acting in the 2D plane,  $\mathbf{E} = \mathbf{E}_0(t) + \mathbf{E}_1(t, \mathbf{r})$  is given by the sum of the homogeneous field of circularly polarized incoming radiation,  $\mathbf{E}_0(t) = E_0(\cos\omega t, -\sin\omega t) = (E_0/2)(\mathbf{e}_x - i\mathbf{e}_y) \exp[-i\omega t] + c.c.$  and the dipole field

$$\mathbf{E}_1(\mathbf{r}, t) = -e\nabla \frac{\mathbf{r}\mathbf{p}(t)}{(r^2 + a^2)^{3/2}}, \quad (4)$$

where  $\mathbf{p}(t) = p(\cos\omega t, -\sin\omega t)$  and  $ep = E_0R^3$  is the dipole moment of a metallic nanosphere with radius  $R$ . (Alternatively, one can use dielectric nanospheres with dielectric constant  $\epsilon_R$ . Then, the dipole moment becomes  $ep = E_0R^3(\epsilon_R + \epsilon)/(\epsilon_R + 2\epsilon)$ , where  $\epsilon$  is the dielectric constant of the transparent embedding matrix [53].) Here, we assume that internal plasmonic frequency of the nanospheres is very large as compared to characteristic frequencies of the problem, so that spheres are fully polarized (corresponding estimates are given in Section VB). For a lattice of the nanospheres, one should replace  $\mathbf{E}_1(\mathbf{r}, t) \rightarrow \sum_i \mathbf{E}_1(\mathbf{r} - \mathbf{r}_i, t)$ , where summation is taken over the lattice nodes.

### B. Rectification of the optical signal

The incoming radiation leads to the oscillations of the concentration and velocity, which are rectified due to the nonlinearity of the hydrodynamic equations. The small signal solution of hydrodynamic equations Eqs. (2) and (3) can be found perturbatively by expansion over  $E_0$  up to the second order

$$n \approx \delta n(t, \mathbf{r}) + \bar{n}(\mathbf{r}), \quad \mathbf{v} \approx \delta \mathbf{v}(t, \mathbf{r}) + \bar{\mathbf{v}}(\mathbf{r}),$$

where  $\delta n(t, \mathbf{r}) \propto E_0$  and  $\delta \mathbf{v}(t, \mathbf{r}) \propto E_0$  are oscillations of the concentration and velocity representing linear response, and  $\bar{n}(\mathbf{r}) \propto E_0^2$  and  $\bar{\mathbf{v}}(\mathbf{r}) \propto E_0^2$  are time-independent corrections arising due to the rectification. We will see that the optically-induced flow of the 2DEL with nonzero vorticity appears even in an ideal liquid with zero viscosity. Therefore, we will first put  $\nu = 0$  and discuss the viscosity related effects at the end of the paper. One of our main findings is that a finite viscosity leads to a very simple contribution to the width of the plasmonic resonances and could be extracted from the measurements of the resonance width.

Due to the rectification, the impinging radiation induces both a dc current  $\mathbf{j}_{\text{dc}}$  and a static electric potential  $\phi_{\text{dc}}$ . To find the rectified corrections  $\bar{n}(\mathbf{r})$  and  $\bar{\mathbf{v}}(\mathbf{r})$  (squared-in- $E_0$ ) we average Eqs. (2) and (3) over time

thus arriving at the following set of the stationary equations

$$\text{div} \bar{\mathbf{v}} = -\text{div} \mathbf{J}_1, \quad (5)$$

$$\gamma \bar{\mathbf{v}} + s^2 \nabla \bar{n} = \gamma \mathbf{J}_2 \quad (6)$$

with the rectified sources. (We neglect terms of the order  $E_0^2$  oscillating at the frequency  $2\omega$ . Such terms leads to negligible, on the order of  $E_0^4$ , corrections to the circular dc current.)

$$\mathbf{J}_1 = \langle \delta n \delta \mathbf{v} \rangle_t, \quad \mathbf{J}_2 = -\frac{1}{\gamma} \langle (\delta \mathbf{v} \nabla) \delta \mathbf{v} \rangle_t. \quad (7)$$

To find total radiation-induced dc current,  $\mathbf{j}_{\text{dc}}$ , one should sum  $\bar{\mathbf{v}}$  and the rectified source  $\mathbf{J}_1$ . The radiation-induced potential,  $\phi_{\text{dc}}$  which creates static electric field  $E_{\text{dc}} = -\nabla \phi_{\text{dc}}$  is found from the condition  $e\nabla \phi_{\text{dc}}/m = s^2 \nabla \bar{n}$ . Thus, we have the following set of equations for  $\mathbf{j}_{\text{dc}}$  and  $\phi_{\text{dc}}$ .

$$\mathbf{j}_{\text{dc}}(\mathbf{r}) = N_0 [\bar{\mathbf{v}}(\mathbf{r}) + \mathbf{J}_1(\mathbf{r})], \quad (8)$$

$$e\phi_{\text{dc}}(\mathbf{r}) = m s^2 \bar{n}(\mathbf{r}). \quad (9)$$

Hence, the key steps of the calculation are as follows. One should first linearize hydrodynamic equations (2) and (3) and find the linear response. The next step is to substitute thus found  $\delta n$  and  $\delta \mathbf{v}$  into the expressions for the non-linear sources given by Eq. (7), perform the time averaging and find  $\mathbf{J}_{1,2}$ . Then, one should calculate  $\bar{n}$  and  $\bar{\mathbf{v}}$  by solving Eqs. (5), (6), and, finally, find  $\mathbf{j}_{\text{dc}}$  and  $\phi_{\text{dc}}$  from Eqs. (8) and (9).

### III. LINEAR RESPONSE: DRUDE AND PLASMONIC CONTRIBUTIONS

Since electric field entering right-hand side of Eq. 3, has both homogeneous and inhomogeneous contributions, one can present the velocity oscillations as the sum of the homogeneous Drude excitation and inhomogeneous dipole-induced plasmonic term, while

$$\delta \mathbf{v} = \delta \mathbf{v}^{\text{D}} + \delta \mathbf{v}^{\text{P}}. \quad (10)$$

Corrections to the concentration appear only due to the inhomogeneous perturbation, so that  $\delta n = \delta n^{\text{P}}$ . As we demonstrate below, the presence of these two types of the velocity excitations leads to interference effects, and, as a consequence, to the Fano-like asymmetry of the resonances.

Linearizing Eqs. (2) and (3) and writing  $\delta n = \delta n_{\omega}(\mathbf{r})e^{-i\omega t} + c.c.$ ,  $\delta \mathbf{v} = \delta \mathbf{v}_{\omega}(\mathbf{r})e^{-i\omega t} + c.c.$ , after simple calculations (see Appendix A) we get

$$\delta n_{\omega}(\mathbf{r}) = \Delta Z(\mathbf{r}), \quad (11)$$

$$\delta \mathbf{v}_{\omega}(\mathbf{r}) = \underbrace{i\omega \nabla Z(\mathbf{r})}_{\delta \mathbf{v}_{\omega}^{\text{D}}} + \underbrace{\frac{eE_0(\mathbf{e}_x - i\mathbf{e}_y)}{2m(\gamma - i\omega)}}_{\delta \mathbf{v}_{\omega}^{\text{P}}}, \quad (12)$$

where, for the case of a single nanosphere

$$Z(\mathbf{r}) = -i2\pi l^2 \int \frac{d^2q}{(2\pi)^2} \frac{e^{i\mathbf{q}\mathbf{r}} e^{-i\varphi_{\mathbf{q}}} e^{-qa}}{q^2 - k^2}. \quad (13)$$

Here  $e^{-i\varphi_{\mathbf{q}}} = (q_x - iq_y)/q$ ,

$$l^2 = \frac{e^2 p}{2ms^2}, \quad (14)$$

and

$$k = \frac{\sqrt{\omega(\omega + i\gamma)}}{s} = k_0 + iQ. \quad (15)$$

The real and imaginary parts of  $k$ , respectively,  $k_0$  and  $Q$ , have a physical meaning of the wave vector and the spatial decrement of the optically excited plasma wave. In what follows, we assume  $\gamma \ll \omega$ . Hence,  $k \approx (\omega + i\gamma/2)/s$ , and, consequently,  $k_0 \approx \omega/s$ ,  $Q \approx \gamma/2s$ . As seen, the spatial decrement of the wave is small

$$Q \ll k_0. \quad (16)$$

For the case of square dipole lattice with the lattice constant  $d$ , Eq. (13) is slightly modified by the replacement (see Appendix E)

$$\int \frac{d^2q}{(2\pi)^2} \rightarrow \frac{1}{d^2} \sum_{\mathbf{q}},$$

where wave vector  $\mathbf{q}$  runs over the inverse lattice vectors

$$\mathbf{q}_{nm} = \frac{2\pi}{d} (n\mathbf{e}_x + m\mathbf{e}_y) \quad (17)$$

Since velocity is given by the sum of two terms [see Eq. (10)], one can split both of the rectified sources  $\mathbf{J}_{1,2}$  into two contributions—the plasmonic contribution and the mixed (plasmonic+Drude) contribution:

$$\mathbf{J}_i = \mathbf{J}_i^{\text{P}} + \mathbf{J}_i^{\text{M}} \quad (i = 1, 2),$$

where

$$\begin{aligned} \mathbf{J}_1^{\text{P}} &= \langle \delta n^{\text{P}} \delta \mathbf{v}^{\text{P}} \rangle_t, \quad \mathbf{J}_2^{\text{P}} = -\frac{\langle (\delta \mathbf{v}^{\text{P}} \nabla) \delta \mathbf{v}^{\text{P}} \rangle_t}{\gamma}, \\ \mathbf{J}_1^{\text{M}} &= \langle \delta n^{\text{P}} \delta \mathbf{v}^{\text{D}} \rangle_t, \quad \mathbf{J}_2^{\text{M}} = -\frac{\langle (\delta \mathbf{v}^{\text{D}} \nabla) \delta \mathbf{v}^{\text{P}} \rangle_t}{\gamma}, \end{aligned} \quad (18)$$

Equations Eq. (13) and (18) allow us to clarify basic physics issues in more detail. First of all, as seen, the integral in the r.h.s. of Eq. (13) contains a pole in the denominator, which reflects the plasmonic resonance occurring when  $\omega$  is equal to the frequency of the plasma wave with the wave vector  $q$ . However, the pole is smeared out due to the integration over  $\mathbf{q}$ . The situation is different for a dipole lattice when the integration should be replaced with summation. For small  $\gamma$ , the contributions of the different terms in the sum are well separated

and can give sharp plasmonic resonances. The resonance condition,

$$\omega = \omega_{nm} = (2\pi s/d) \sqrt{n^2 + m^2}, \quad (19)$$

is satisfied for several pairs  $(n, m)$ . For example, the fundamental plasmonic resonance with the frequency

$$\omega_0 = \frac{2\pi s}{d}, \quad (20)$$

corresponds to the sum over 4 pairs  $(1, 0), (-1, 0), (0, 1)$  and  $(0, -1)$  yielding

$$Z_0(\mathbf{r}) \propto \frac{1}{\omega_0^2 - \omega^2 - i\omega\gamma}, \quad (21)$$

with the frequency-independent coefficient of proportionality. Then, rectified dc currents has the resonance dependence  $\mathbf{J}_i^{\text{P}} \propto |Z(\mathbf{r})|^2$ ,  $\mathbf{J}_i^{\text{M}} \propto Z(\mathbf{r})$ . As a result, in the vicinity of the resonance, the expression for the circular dc current can be approximately presented as follows

$$\mathbf{j}_{\text{dc}} \approx \frac{\boldsymbol{\pi}(\mathbf{r})}{\Omega^2 + \Gamma^2/4} + \left[ \frac{\boldsymbol{\mu}(\mathbf{r})}{\Omega + i\Gamma/2} + c.c. \right]. \quad (22)$$

where

$$\Omega = \frac{\omega - \omega_0}{\omega_0}, \quad \Gamma = \frac{\gamma}{\omega_0}, \quad (23)$$

are, respectively, the dimensionless detuning and damping of the fundamental resonance, while the terms proportional to vectors  $\boldsymbol{\pi}(\mathbf{r})$  and  $\boldsymbol{\mu}(\mathbf{r})$  represent the plasmonic and mixed contributions, respectively [exact expressions for these coefficients will be given below, see Eqs. (40), and (41)]. Due to the interference of these terms, the resonance in  $\mathbf{j}_{\text{dc}}$  and  $\phi_{\text{dc}}$ , has an asymmetric Fano-like shape. Interestingly enough, the degree of asymmetry depends on the coordinate  $\mathbf{r}$ .

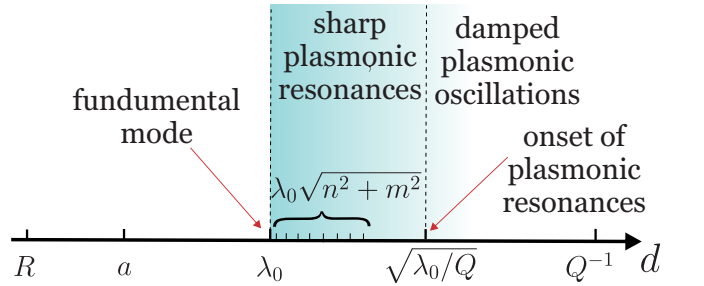


FIG. 2. Different scales of the problem. We predict sharp plasmonic resonances for  $\lambda_0 < d < \sqrt{\lambda_0/Q}$ .

Different scales of the problem are illustrated in Fig. 2. The smallest scale is the size of the sphere,  $R$ , which is on the order or smaller than the distance from spheres to the plane of 2D gas,  $R \lesssim a$ . We assume that the wavelength of the plasma excitations,  $\lambda_0 = 2\pi/k_0$ , is much larger than  $a$  but smaller than the plasma wave damping length:

$a \ll \lambda_0 \ll Q^{-1}$ . For  $d \gg Q^{-1}$ , the spheres are fully independent and it is sufficient to calculate the response of a single sphere. With decreasing  $d$ , the spheres begin to influence each other. One can easily estimate characteristic  $d$  corresponding to onset of plasmonic resonances. To this end, we estimate the volume in the momentum space corresponding to a plasmonic resonance as  $k_0 Q$ . When this volume becomes smaller than the volume of the unit cell of the inverse lattice,  $k_0 Q \ll (2\pi/d)^2$  the resonances cease to overlap. The fundamental mode corresponds to a smaller inter-sphere distance:  $d = \lambda_0$ . The total number of well resolved resonances that can be observed is proportional to  $k_0/Q = \omega/\gamma$  and is thus determined by the quality factor. It is worth noting that sharp resonances exist in the finite range of  $d$ :  $\lambda_0 \lesssim d \lesssim \sqrt{\lambda_0/Q}$ .

An important comment is related to the radiation-induced vorticity of the 2DEL. On the formal level, function  $Z(\mathbf{r})$  is a Green's function of hydrodynamic equations describing the plasmonic excitation caused by a point-like rotating dipole. Due to this rotation, an angular momentum  $\pm 1$  is transferred to the liquid with the sign determined by the sign of the helicity. The information about this moment is encoded in the phase factor  $\exp[-i\varphi_{\mathbf{q}}]$  in Eq. (13). This means that the plasma waves circulate around the nanospheres and that direction of circulation changes with changing the sign of the radiation polarization. We call such excitations "twisted plasmons". The rectification of these plasmons leads to dc current with non-zero vorticity, which is also determined by the helicity sign.

#### IV. CIRCULAR DC CURRENT INDUCED BY A SINGLE DIPOLE

Performing integration over  $\varphi_{\mathbf{q}}$  in Eq. (13), we get

$$Z(\mathbf{r}) = l^2(x - iy)f(r), \quad (24)$$

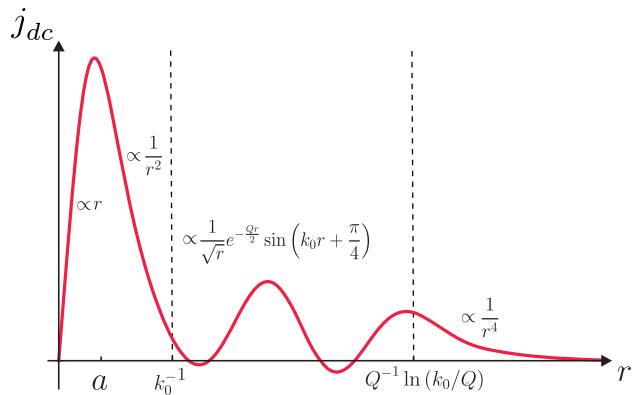


FIG. 3. Dependence of the circular current density,  $j_{\text{dc}}$ , created in 2D liquid by a rotating dipole moment of a single nanosphere. Main contribution to this current comes from mixed term [See Eq. (28)]

where function  $f$  depends only on  $r = |\mathbf{r}|$ . The analytical expressions for  $f$  and its asymptotes are presented in the Appendix A together with expression of  $\delta n_{\omega}$  and  $\delta v_{\omega}$  in terms of  $f$ . It is convenient to present  $\mathbf{J}_i$  as follows

$$\mathbf{J}_i = R_i \mathbf{e}_r + \Phi_i \mathbf{e}_{\varphi}, \quad (25)$$

where  $\mathbf{e}_r = \mathbf{r}/r$ ,  $\mathbf{e}_{\varphi} = \mathbf{e}_z \times \mathbf{e}_r$  and functions  $R_i = R_i^P + R_i^M$ , and  $\Phi_i = \Phi_i^P + \Phi_i^M$ , depend only on  $r = |\mathbf{r}|$  and contain both plasmonic and mixed contributions. Here, vector  $\mathbf{r}$  is counted from the center of nanosphere (see Fig. 1a).

Provided that  $R_i$  and  $\Phi_i$  are known, the solution of Eqs. (5) and (6) can be found by expanding  $\bar{\mathbf{v}}$  over  $\mathbf{e}_r$  and  $\mathbf{e}_{\varphi}$  and assuming  $\bar{n} = \bar{n}(r)$ . We find for the total circular radiation-induced dc current,  $\mathbf{j}_{\text{dc}} = j_{\text{dc}} \mathbf{e}_{\varphi}$  and the radial electric field,  $E_{\text{dc}} = E_{\text{dc}} \mathbf{e}_r$ :

$$j_{\text{dc}} = N_0(\Phi_1 + \Phi_2) \quad (26)$$

$$\frac{eE_{\text{dc}}}{m} = \gamma(R_1 + R_2) \quad (27)$$

Expressions for plasmonic and mixed contributions,  $R_i^P, \Phi_i^P$  and  $R_i^M, \Phi_i^M$ , are presented in Appendixes B and C, respectively, as well as expressions for asymptotical behavior of  $j_{\text{dc}}$  [see Eq. (D1)] and  $E_{\text{dc}}$  [see Eq. (D2)] accounting for both plasmonic and mixed contribution. As seen, for the most realistic case ( $R \ll a \ll k_0^{-1} \ll Q^{-1}$ ), the mixed contribution dominates. Neglecting plasmonic contribution, we find that

$$j_{\text{dc}} \approx -j_* \begin{cases} C \left( \frac{r}{a} \right), & r \ll 1/k_0, \\ \frac{\sqrt{2\pi} k_0^{3/2} a^2}{\sqrt{r}} e^{-Qr/2} \sin(k_0 r + \pi/4), & 1/k_0 \ll r \ll \frac{\ln[k_0/Q]}{Q}, \\ \frac{6a^2}{k_0^2 r^2}, & \frac{\ln[k_0/Q]}{Q} \ll r \end{cases}, \quad (28)$$

where

$$j_* = \frac{\omega l^4 N_0}{k_0^2 R^3 a^2}, \quad (29)$$

and  $C(x)$  is given by Eq. (D4). Schematic dependence of  $j_{\text{DC}}$  on  $r$  is shown in Fig. (3). The static optically-induced field is linked to the dc circular current by a simple relation

$$j_{\text{dc}} = -\frac{eE_{\text{dc}}N_0}{m\omega}. \quad (30)$$

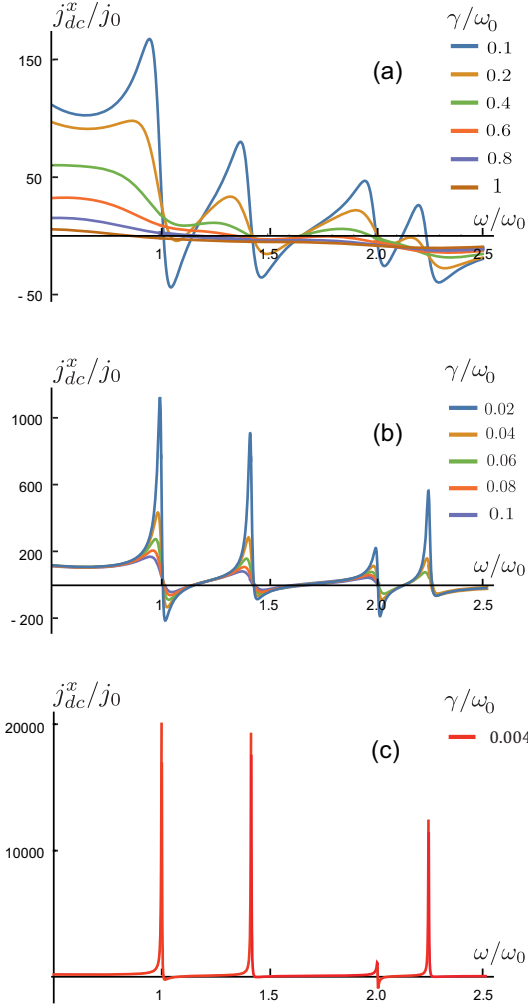


FIG. 4. Frequency dependence of  $x$ - component of the current density for  $x = y = d/8$ ,  $R = a/2$ ,  $d = 5a$ : onset of plasmonic resonances at large  $\gamma$  (a); strongly asymmetric resonances at intermediate values of  $\gamma$  (b); weakly asymmetric resonances at very small  $\gamma$  (c).

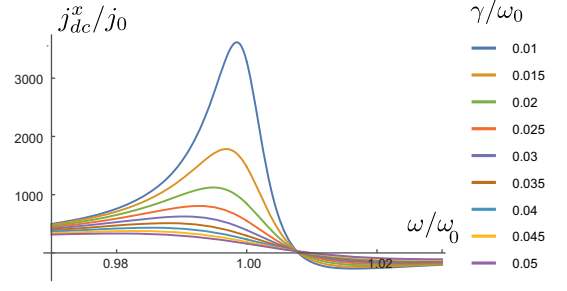


FIG. 5. Fundamental plasmonic peak in  $x$  component of dc current for  $x = y = d/8$ ,  $R = a/2$ ,  $d = 5a$  and different values of  $\gamma$ . The asymmetry of the peak decreases with decreasing of  $\gamma$ .

### A. Dipole lattice

For a lattice of dipoles, we write the Fourier components of the nonlinear sources  $\mathbf{J}_1$  and  $\mathbf{J}_2$  as follows

$$\mathbf{J}_{i\mathbf{q}\omega} = R_{i\mathbf{q}} \mathbf{n}_{\mathbf{q}}^{\parallel} + \Phi_{i\mathbf{q}} \mathbf{n}_{\mathbf{q}}^{\perp}, \quad i = (1, 2) \quad (31)$$

where  $\mathbf{n}_{\mathbf{q}}^{\parallel} = \mathbf{q}/q$  and  $\mathbf{n}_{\mathbf{q}}^{\perp} = \mathbf{e}_z \times \mathbf{q}/q$ . The Fourier transform of Eqs. (5) and (6) yields expressions similar to Eqs. (26) and Eq. (27):

$$\mathbf{j}_{\mathbf{q}}^{\text{dc}} = N_0(\Phi_{1\mathbf{q}} + \Phi_{2\mathbf{q}})\mathbf{n}_{\mathbf{q}}^{\perp}, \quad (32)$$

$$\frac{e\mathbf{E}_{\mathbf{q}}^{\text{dc}}}{m} = \gamma(R_{1\mathbf{q}} + R_{2\mathbf{q}})\mathbf{n}_{\mathbf{q}}^{\parallel}. \quad (33)$$

The Fourier components of the dc current and static field can be presented as sums over the plasmonic and mixed contributions:  $R_{i\mathbf{q}} = R_{i\mathbf{q}}^{\text{P}} + R_{i\mathbf{q}}^{\text{M}}$ ,  $\Phi_{i\mathbf{q}} = \Phi_{i\mathbf{q}}^{\text{P}} + \Phi_{i\mathbf{q}}^{\text{M}}$ .

We consider the simplest case of a square lattice with the lattice constant  $d$ . In this case, all the integrals over  $\mathbf{q}$  should be replaced with the sums over the vectors of the inverse lattice [see Eq. (17)] and function  $Z(\mathbf{r})$  becomes

$$Z(\mathbf{r}) = -\frac{i2\pi l^2}{d^2} \sum_{\mathbf{q}} \frac{e^{i\mathbf{q}\mathbf{r}}}{q^2 - k^2} e^{-i\varphi_{\mathbf{q}}} e^{-q a}. \quad (34)$$

Using this equation, we find

$$\delta n_{\omega} = \frac{2i\pi l^2}{d^2} \sum_{\mathbf{q}} \frac{e^{i\mathbf{q}\mathbf{r}} e^{-i\varphi_{\mathbf{q}}} q^2 e^{-q a}}{q^2 - k^2}, \quad (35)$$

$$\delta \mathbf{v}_{\omega} = \frac{2i\pi l^2}{d^2} \sum_{\mathbf{q}} \frac{e^{i\mathbf{q}\mathbf{r}} e^{-i\varphi_{\mathbf{q}}} \omega \mathbf{q} e^{-q a}}{q^2 - k^2} + \frac{eE_0(\mathbf{e}_x - i\mathbf{e}_y)}{2m(\gamma - i\omega)}. \quad (36)$$

The rectified currents  $\mathbf{J}_i^{\text{P,M}}$  can be calculated using Eqs. (18), (35), and (36). Corresponding analytical expressions are given in Appendix E. Resulting equations for  $\mathbf{j}_{\text{dc}}$  and  $\mathbf{E}_{\text{dc}}$  are given, respectively, by Eqs. (E9) and (E10).

In Fig. 4 we plotted the  $x$ -component of the dc current in units of

$$j_0 = N_0 \frac{4\pi^2 l^4 s}{d^4},$$

in a certain point in the plane (we used  $x = y = d/8$ ) as a function of the radiation frequency for different damping rates (picture for the  $y$  component of the current looks analogous). As seen, with decreasing the  $\gamma$ , sharp resonances appear on the top of the smooth dependence. Due to the interference of the plasmonic and mixed contributions, the resonances have an asymmetric shape. The degree of asymmetry is smaller for small  $\gamma$ , because the symmetric plasmonic contribution dominates at  $\gamma \rightarrow 0$ . Fig. 5 illustrates the asymmetry of the peaks for fundamental mode. To demonstrate vorticity of the current, we also plotted the calculated current vector density in Fig. 6.

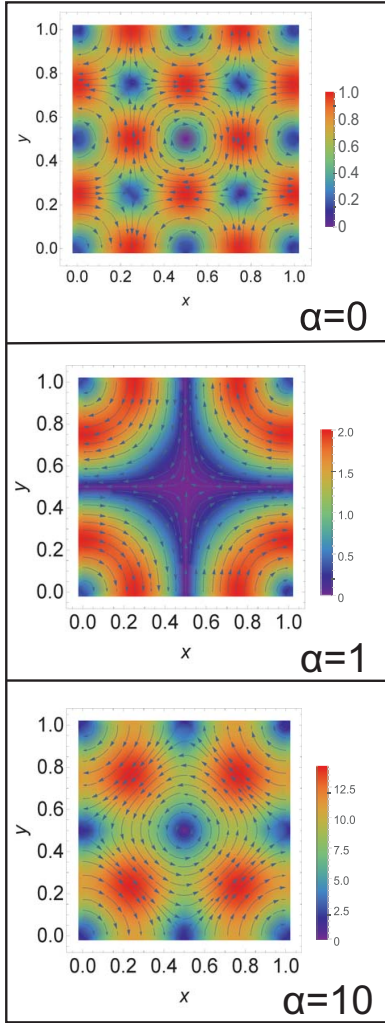


FIG. 6. Vector density plot of the rectified current density  $\mathbf{j}_{dc}$  for different values of parameter  $\alpha = 2\Omega\mu_0/\pi_0$ . (here,  $x$  and  $y$  are measured in units of  $d$ )

## B. Excitation of the fundamental mode

The smallest resonant frequency,  $\omega_0$ , is given by Eq. (20). This frequency corresponds to the contribution of four terms, with

$$(n, m) = (1, 0), (0, 1), (-1, 0), (0, -1). \quad (37)$$

For all these terms we have  $q = q_0 = 2\pi/d$ . The frequency of the next resonance is given by  $\sqrt{2}\omega_0$ . It corresponds to other four terms with  $(n, m) = (\pm 1, \pm 1)$ . For sufficiently high quality factors,

$$\omega_0/\gamma \gg 1,$$

these two resonances are well separated. Hence, for  $\omega$  close to  $\omega_0$ , only four terms corresponding to Eq. (37) contribute to the sum over  $\mathbf{q}_{nm}$ , while terms with other  $n$  and  $m$  can be neglected (this corresponds to the resonance approximation).

Within the resonance approximation, the concentration and velocity are given by

$$\begin{aligned} \delta n_\omega &= \frac{4\pi l^2}{d^2} \frac{q_0^2 e^{-q_0 a} [i \sin(q_0 y) - \sin(q_0 x)]}{q_0^2 - k^2}, \quad (38) \\ \delta \mathbf{v}_\omega &= \frac{4\pi l^2}{d^2} \frac{\omega q_0 e^{-q_0 a} [i \mathbf{e}_x \cos(q_0 x) + \mathbf{e}_y \cos(q_0 y)]}{q_0^2 - k^2} \\ &\quad + \frac{e E_0 (\mathbf{e}_x - i \mathbf{e}_y)}{2m(\gamma - i\omega)}, \quad (39) \end{aligned}$$

Using the equations given in Appendix F, we find that the circular current can be presented in the form of Eq. (22), with

$$\boldsymbol{\pi}(\mathbf{r}) = \pi_0 [\sin(q_0 y) \cos(q_0 x) \mathbf{e}_x \quad (40)$$

$$- \sin(q_0 x) \cos(q_0 y) \mathbf{e}_y],$$

$$\boldsymbol{\mu}(\mathbf{r}) = \mu_0 [\sin(q_0 y) \mathbf{e}_x - \sin(q_0 x) \mathbf{e}_y], \quad (41)$$

where

$$\pi_0 = \frac{8\pi^2 N_0 s l^4}{d^4} e^{-2q_0 a}, \quad \mu_0 = \frac{N_0 s l^4}{d R^3} e^{-q_0 a} \quad (42)$$

As seen,  $\text{div} \boldsymbol{\pi} = \text{div} \boldsymbol{\mu} = 0$ , so that  $\mathbf{j}_{dc}$  is purely circular current,  $\text{div} \mathbf{j}_{dc} = 0$ , with non-zero vorticity:

$$\begin{aligned} \nabla \times \mathbf{j}_{dc} &= -\mathbf{e}_z \frac{2q_0}{\Omega^2 + \Gamma^2/4} \quad (43) \\ &\quad \times \{ \pi_0 \cos(q_0 x) \cos(q_0 y) \\ &\quad + \mu_0 \Omega [\cos(q_0 x) + \cos(q_0 y)] \}. \end{aligned}$$

Two interfering contributions, plasmonic and mixed, have different frequency dependencies in the vicinity of the resonance, symmetric and asymmetric ones, respectively. Interestingly, the degree of asymmetry depends on coordinate. For example, at the line  $\cos(q_0 x) + \cos(q_0 y) = 0$  the vorticity is a symmetric function of  $\Omega$ , while for  $\cos(q_0 x) = 0$  or  $\cos(q_0 y) = 0$ , the vorticity is described by an asymmetric mixed term. The vector density plot

of the rectified current  $j_{dc}$  is plotted in Fig. 6 for different values of parameter

$$\alpha = \frac{2\Omega\mu_0}{\pi_0} = \frac{d^3\Omega}{4\pi^2 R^3} e^{q_0 a}, \quad (44)$$

which depends on the dimensionless deviation from the resonance,  $\Omega$ . Hence, changing radiation frequency, one can qualitatively change the spatial distribution of dc current. In order to understand this dependence better, we rewrite Eq. (22) as follows

$$\begin{aligned} \frac{j_{dc}}{j_0} &= \frac{2e^{-2q_0 a}}{\Omega^2 + (\Gamma/2)^2} \{ \mathbf{e}_x \sin(q_0 y) [\alpha + \cos(q_0 x)] \\ &- \mathbf{e}_y \sin(q_0 x) [\alpha + \cos(q_0 y)] \}. \end{aligned} \quad (45)$$

As seen, the key parameter which determines the current distribution is  $\alpha$ . Below, we will analyze the vector structure of this equation. For brevity, we skip common coefficient  $2j_0 e^{-2q_0 a} / [\Omega^2 + (\Gamma/2)^2]$  in the expressions for current.

For  $\alpha \ll 1$ , we get

$$\begin{aligned} j_{dc} &\propto \mathbf{e}_x \sin(q_0 y) \cos(q_0 x) - \mathbf{e}_y \sin(q_0 x) \cos(q_0 y) \\ j_{dc}^2 &\propto \frac{1 - \cos(2q_0 x) \cos(2q_0 y)}{2}. \end{aligned}$$

From these equations we find that the current reaches its maximum absolute value at points  $\mathbf{r}_{nm}^I = (x_n^I, y_m^I) = (d/2)(n + 1/2, m)$  and  $\mathbf{r}_{nm}^{II} = (x_n^{II}, y_m^{II}) = (d/2)(n, m + 1/2)$  (here and below  $n$  and  $m$  are integer numbers). These points correspond to centers of red circles in Fig. 6a. From Eq. (45) we find values of currents,  $j_{dc}^I$  and  $j_{dc}^{II}$ , exactly at  $\mathbf{r}^I$  and  $\mathbf{r}^{II}$ , respectively, and their variations,  $\delta j_{dc}^I$ ,  $\delta j_{dc}^{II}$ , in the vicinity of these points

$$\begin{aligned} j_{dc}^I &\propto -\mathbf{e}_y (-1)^{n+m}, \\ \delta j_{dc}^I &\propto (-1)^{n+m} q_0^2 \left( \mathbf{e}_y \frac{\delta x^2 + \delta y^2}{2} - \mathbf{e}_x \delta x \delta y \right), \\ j_{dc}^{II} &\propto \mathbf{e}_x (-1)^{n+m}, \\ \delta j_{dc}^{II} &\propto (-1)^{n+m} q_0^2 \left( -\mathbf{e}_x \frac{\delta x^2 + \delta y^2}{2} + \mathbf{e}_y \delta x \delta y \right). \end{aligned}$$

Here,  $\delta \mathbf{r} = (\delta x, \delta y)$  is a small deviation of  $\mathbf{r}$  from point  $\mathbf{r}^I$  or  $\mathbf{r}^{II}$  ( $q_0 \delta r \ll 1$ ). Analyzing these equations and Fig. 6a, we see that there are 8 current maxima (per unit cell of arising periodic structure) with different current behavior. Here  $\delta x$  and  $\delta y$  are counted from  $\mathbf{r}^I$  or  $\mathbf{r}^{II}$ . For  $\alpha \gg 1$ , we find that the current is given by

$$\begin{aligned} j_{dc} &\propto \alpha [\mathbf{e}_x \sin(q_0 y) + \mathbf{e}_y \sin(q_0 x)], \\ j_{dc}^2 &\propto \alpha^2 [\sin^2(q_0 y) + \sin^2(q_0 x)]. \end{aligned}$$

We see that dependencies on  $x$  and  $y$  fully decouple. The current is maximal at points  $(x_n, y_m) = (d/2)(n + 1/2, m + 1/2)$ , corresponding to centers of the red circles

in Fig. 6c. Close to these points, we get

$$\begin{aligned} j_{dc} &\propto (-1)^m \alpha \mathbf{e}_x \left( 1 - \frac{q_0^2 \delta y^2}{2} \right) \\ &+ (-1)^n \alpha \mathbf{e}_y \left( 1 - \frac{q_0^2 \delta x^2}{2} \right). \end{aligned} \quad (46)$$

Hence, in this case there are four maxima with different current behavior per unit cell of the periodic current structure.

The vector density plots for  $\alpha \ll 1$  and  $\alpha \gg 1$  are essentially different. The transition between these plots happens at  $\alpha \sim 1$ . Let us consider, for example, the quadrant of the unit cell of the periodic structure of the current, corresponding to  $0 < x < d/2$  and  $0 < y < d/2$  (behavior in the remaining three quadrants can be considered analogously). For  $\alpha = 0$ ,  $j_{dc}^2$  has four maxima of equal heights at the points  $\mathbf{r}_{00}^I, \mathbf{r}_{00}^I, \mathbf{r}_{01}^I$  and  $\mathbf{r}_{10}^I$  [see Fig. 6a]. With increasing  $\alpha$  first two maxima increase by a factor  $(1 + \alpha)^2$ , while the second two decrease by a factor  $(1 - \alpha)^2$ . Also, for  $\alpha < \sqrt{8/3}$  there is a saddle point in this quadrant at

$$x = y = \frac{d}{2\pi} \arccos \left( \frac{2}{\alpha + \sqrt{\alpha^2 + 8}} \right). \quad (47)$$

The squared current at the saddle point is

$$j_{dc}^2 \propto \frac{4(2 + a(a + \sqrt{8 + a^2}))^3}{(a + \sqrt{8 + a^2})^4}. \quad (48)$$

At  $\alpha > \sqrt{8/3}$ , the saddle point transforms to a maximum and the amplitude of this maximum becomes higher than for the maxima at points  $\mathbf{r}_{00}^I, \mathbf{r}_{00}^I$ . With a further increase of  $\alpha$  the new maximum moves to the point  $(x, y) = (d/4, d/4)$ , and stops at this position for  $\alpha \rightarrow \infty$ . The behavior of current in the vicinity of this maximum at  $\alpha \gg 1$  is described by Eq. (46). It is also worth noticing that for  $\alpha \sim 1$  the value given by Eq. (48) is close to the value of maxima at points  $\mathbf{r}_{00}^I, \mathbf{r}_{00}^I$ . Therefore, the vector density plot shows red circular band (see Fig. 6b).

Analogously, one can calculate the optically-induced static potential

$$\begin{aligned} \frac{e\phi_{dc}}{m} &= \frac{2\pi^2 l^4 s^2}{d^4} \frac{e^{-2q_0 a}}{\Omega^2 + \Gamma^2/4} \\ &\times \{ \cos(2q_0 x) + \cos(2q_0 y) \\ &- 4\alpha [\cos(q_0 x) + \cos(q_0 y)] \}. \end{aligned} \quad (49)$$

As one can see from this equation, the maximal optically induced voltage drop across different points of the unit cell of the periodic voltage structures is proportional to the amplitude of the circulating dc current  $e\delta\phi_{dc}^{\max} \sim j_{dc} s / N_0$ .



### C. Optically-induced magnetic field

The stationary radiation-induced magnetic field obeys

$$[\nabla \times \mathbf{H}] = \frac{4\pi e \mathbf{j}_{\text{dc}}(\mathbf{r})}{c} \delta(z). \quad (50)$$

Substituting  $\mathbf{H} = [\nabla \times \mathbf{A}]$  ( $\text{div} \mathbf{A} = 0$ ) and making Fourier transform over  $\mathbf{r}$ , we find

$$k^2 \mathbf{A}_{\mathbf{k}} - \frac{d^2 \mathbf{A}_{\mathbf{k}}}{dz^2} = \frac{4\pi e \mathbf{j}_{\text{dc}}^{\mathbf{k}}}{c} \delta(z). \quad (51)$$

Finite at  $|z| \rightarrow \infty$  solution of this equation reads  $\mathbf{A}_{\mathbf{k}}(z) = (2\pi e/c\mathbf{k}) \mathbf{j}_{\text{dc}}^{\mathbf{k}} \exp(-k|z|)$ . Hence, the Fourier transform of the vector potential (and, consequently, of the magnetic field) is proportional to the Fourier transform of the dc current. In the vicinity of plasmonic peaks, only several  $\mathbf{k}$  satisfying resonant conditions contribute to the current and magnetic field, so that spatial dependence of the field is found by the summation over these discrete set of  $\mathbf{k}$ .

Let us, for example, calculate the perpendicular component of the field,  $H_z$ , in the fundamental mode within the resonance approximation. In this case,  $\mathbf{k}$  runs over  $(\pm q_0, \pm q_0)$  for the plasmonic contribution and over  $(\pm q_0, 0)$  and  $(0, \pm q_0)$  for the mixed contribution [see Eqs. (40) and (41)]. Instead of summation over these  $\mathbf{k}$ , one can take into account that all terms in  $\pi(\mathbf{r})$  and  $\mu(\mathbf{r})$  are eigenfunctions of the Laplace operator,  $\Delta$ , and present the field in the operator form as

$$H_z(\mathbf{r}, z) = \frac{e^{-\sqrt{-\Delta}|z|}}{\sqrt{-\Delta}} \frac{2\pi e \mathbf{e}_z [\nabla \times \mathbf{j}_{\text{dc}}(\mathbf{r})]}{c}. \quad (52)$$

From this equation and Eq. (43), we find

$$\begin{aligned} H_z(\mathbf{r}, z) = & -\frac{4\pi e}{c} \frac{1}{\Omega^2 + \Gamma^2/4} \\ & \times \left\{ \pi_0 \cos(q_0 x) \cos(q_0 y) \frac{e^{-\sqrt{2}q_0|z|}}{\sqrt{2}} \right. \\ & \left. + \mu_0 \Omega [\cos(q_0 x) + \cos(q_0 y)] e^{-\sqrt{q_0}|z|} \right\}. \end{aligned} \quad (53)$$

Figure (7) shows the density plot of the magnetic field in the 2DEL plane:

$$\begin{aligned} H_z(\mathbf{r}, 0) = & -\frac{\sqrt{32}\pi e j_0}{c} \frac{e^{-2q_0 a}}{\Omega^2 + \Gamma^2/4} \left\{ \cos(q_0 x) \cos(q_0 y) \right. \\ & \left. + \frac{\alpha}{\sqrt{2}} [\cos(q_0 x) + \cos(q_0 y)] \right\}. \end{aligned} \quad (54)$$

For  $\alpha \ll 1$ , the field has maxima (within the area  $0 < x < d$ ,  $0 < y < d$ ) at the points  $(0, 0)$ ,  $(d, 0)$ ,  $(0, d)$ ,  $(d/2, d/2)$ ,  $(d, d)$  where  $\cos(q_0 x) \cos(q_0 y)$  is maximal (these maxima have equal heights and correspond to centers of red circles in Fig. 7a). With increasing  $\alpha$ , the amplitude of the central maximum at  $(d/2, d/2)$  decreases by the factor  $1 - 2\alpha$

(for  $\alpha > 1$  this maximum transforms into minimum), while the amplitude of other four maxima is increased by the factor  $1 + 2\alpha$ . Hence, for  $\alpha \gg 1$ , the field has four equivalent maxima at the points  $(0, 0)$ ,  $(d, 0)$ ,  $(0, d)$ ,  $(d, d)$  corresponding to the maxima of both  $\cos(q_0 x) + \cos(q_0 y)$  and  $\cos(q_0 x) \cos(q_0 y)$  (the maxima correspond to centers of red circles in Fig. 7c).

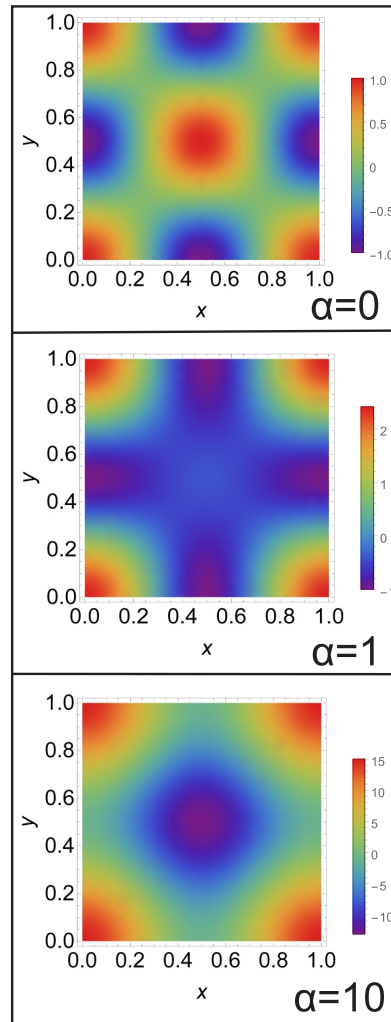


FIG. 7. Density plot of  $H_z(\mathbf{r}, 0)$  for different values of parameter  $\alpha = 2\Omega\mu_0/\pi_0$  (here,  $x$  and  $y$  are measured in units of  $d$ )

## V. DISCUSSION

### A. Finite viscosity, external magnetic field and finite size effects.

Above, we presented calculations for zero external magnetic field for an ideal infinite 2DEL with zero viscosity. The detailed analysis of different magnetoresistance regimes of the viscous electron liquid in the system un-

der discussion is out of scope of this work and will be presented elsewhere. Here, we limit ourselves to the simplest but at the same time the most interesting case of the resonant excitation, when some of the plasmonic modes with wavevectors given by Eq. (17) satisfy the resonance condition:  $\omega \approx \omega_{nm}$ , where  $\omega_{nm}$  is given by Eq. (19). In this case, within the resonant approximation, the effect of a weak magnetic field,  $B$ , with  $\omega_c \ll \omega$  ( $\omega_c = eB/mc$  is the cyclotron frequency) can be accounted for by replacing  $\omega_{nm}^2$  with

$$\omega_{nm}^2(B) = \omega_{nm}^2 + \omega_c^2. \quad (55)$$

Hence, a weak magnetic field shifts the positions of the resonances shown in Fig. 4 thus giving an additional way to control the dc current and magnetization.

Within the same resonance approximation, the effect of a weak viscosity, satisfying the inequality  $\nu q_{nm}^2 \ll \omega$ , is accounted by replacing elastic damping  $\gamma$  with

$$\gamma_{nm} = \gamma + \nu q_{nm}^2. \quad (56)$$

The resonance is described by Eq. (22) with

$$\Omega \approx \frac{\omega - \omega_{nm}(B)}{\omega_{nm}(B)}, \quad \Gamma \approx \frac{\gamma_{nm}}{\omega_{nm}}. \quad (57)$$

As seen from Eq. (56), the measurement of widths of two plasmonic resonances with different resonance frequencies ( $\omega_{n_1 m_1} \neq \omega_{n_2 m_2}$ ) allows one to extract value of  $\nu$ :

$$\nu = \frac{(\gamma_{n_1 m_1} - \gamma_{n_2 m_2})d^2}{(2\pi)^2(n_1^2 + m_1^2 - n_2^2 - m_2^2)}. \quad (58)$$

Evidently, one can also extract the momentum relaxation time by measuring  $\gamma_{n_1 m_1}$  and  $\gamma_{n_2 m_2}$ . It worth noting that Eq. (58) does not include any characteristic of the material and depends on a single geometrical factor—the distance between nanospheres, which can be well controlled in experiment. Hence, the HIFE gives a direct way to extract the electron viscosity.

In this paper, we considered an infinite 2D system. An interesting question is related to finite size effects, i.e. to the behavior of the current and magnetic field at the boundary of the system. A detailed discussion of this issue is beyond the scope of this work and will be studied elsewhere. Here we restrict ourselves to a few comments. One can consider the situation when a diffraction square lattice having a finite size  $L = Nd$ , (here  $N \gg 1$  is an integer number) is located over an infinite 2D plane. Then, when calculating the function  $Z(\mathbf{r})$  in integrals over  $dq_i$  ( $i = x, y$ ), the factors  $\sin(q_i L/2)/\sin(q_i d/2)$  appear, which describe the smearing of  $\mathbf{q}$  around the quantized vectors of inverse lattice of  $\mathbf{q}_{nm}$  [see Eq. (17)] by values of the order of  $\delta q_i \sim 1/L$ . Considering the fundamental mode and calculating the corresponding integrals, one can show that outside of the region covered by diffraction lattice the plasmonic and mixed contributions exponentially decay with different exponents

$$\pi(\mathbf{r}) \propto \exp(-\delta r/L_\pi), \quad \mu(\mathbf{r}) \propto \exp(-\delta r/L_\mu),$$

where  $\delta r$  is distance from the edge of the diffraction region,  $L_\pi = 1/\sqrt{k_0 Q} = s/\sqrt{\omega_0 \gamma}$ , and  $L_\mu = 1/Q = s/\gamma$ . It is worth noting that for a small damping rate both  $L_\pi$  and  $L_\mu$  might become on the order or even larger than  $L$ , which means that for sufficiently clean 2DEL the circular current and magnetic field can appear well beyond the region covered by diffraction lattice.

## B. Estimates of relevant parameters for various structures

In this Section, we present some estimates of the relevant physical parameters for various materials and briefly discuss applicability of our approximations for realistic structures. We use the following geometrical parameters:  $d = 250$  nm,  $a = 50$  nm,  $R = 25$  nm. The plasma wave velocity is estimated by using standard equation [16] and assuming that there is the back gate in the system. The barrier (spacer) width given in Table I corresponds to the typical values for each material system. The electric field of the incoming radiation is taken as  $E_0 = 10^5$  V/cm. We estimate both current  $j_0$ , which characterize the current flow for non-resonant case, when the quality factor is on the order of unity, and also the current

$$j_{dc}^m = \frac{8j_0}{\Gamma^2} \exp^{-4\pi a/d}, \quad (59)$$

which is much larger than  $j_0$  for sharp resonances, when  $\Gamma \ll 1$  [see Eq. (45)]. For estimates of plasmonic-enhanced magnetic field we use

$$H^m = \frac{16\sqrt{2}\pi e j_0}{c\Gamma^2} \exp^{-4\pi a/d}, \quad (60)$$

[see Eq. (54)].

Table I list the calculated values of the most important parameters, i.e. fundamental frequency, quality factor, characteristic value of the dc current, and maximal magnetic field. For all the materials listed in this Table, the frequency of the fundamental plasmonic mode is in the THz range. The value of optically-induced magnetic field can be sufficiently large at not too low temperature, 77 K, especially in the GaN and p-diamond-based structures. For these estimates we used material parameters listed in Table II with references to corresponding experiments and/or numerical simulations. Using the numbers, presented in the above Tables, we can discuss validity of approximations used in our calculations.

In our model we assumed that the spheres comprising the plasmonic coupler are fully polarized. This implies that internal plasmonic frequency of the nanospheres is very large compared to characteristic frequencies of the problem. The condition is well satisfied provided that frequency of three dimensional plasma oscillations in the metal, which the spheres are made from,  $\omega_{3D}$ , is large as compared to typical plasmonic frequency in our problem, which is the fundamental frequency  $\omega_0$  [see Eq. (20)]. For typical value of plasma wave velocity in 2D gated InGaAs-based structure,  $s \sim 1.6 \times 10^8$  cm/s [16], and  $d =$

250 nm, we get  $f_0 = \omega_0/2\pi = 6.4$  THz (see Table I and Fig. 8). At the same time the 3D plasmonic frequencies in metal are at least two order of magnitude higher due to very high electron concentration. For example, simple estimate for silver, with 3D concentration  $6 \times 10^{22} \text{ cm}^{-3}$ , yields for  $\omega_{3D}$  value about  $10^{16} \text{ s}^{-1}$ .

Let us now estimate spatial scales shown in Fig. 2. Assuming the frequency of the radiation to be  $\omega = 3 \times 10^{13} \text{ s}^{-1}$  (which corresponds to  $f = \omega/2\pi = 5$  THz), and using estimate for typical plasma wave velocity  $1.6 \times 10^8 \text{ cm/s}$  we find  $\lambda_0 = 250$  nm. Rewriting damping length as  $Q^{-1} = \lambda_0(\omega_0/\gamma\pi)$  and using data of Table I for InGaAs at  $T=77$  K, we estimate  $Q^{-1} \approx 3500$  nm. This justifies ordering of the spatial scales in Fig. 2. As seen from

Table I, for other materials we also have  $Q^{-1} \gg \lambda_0$ .

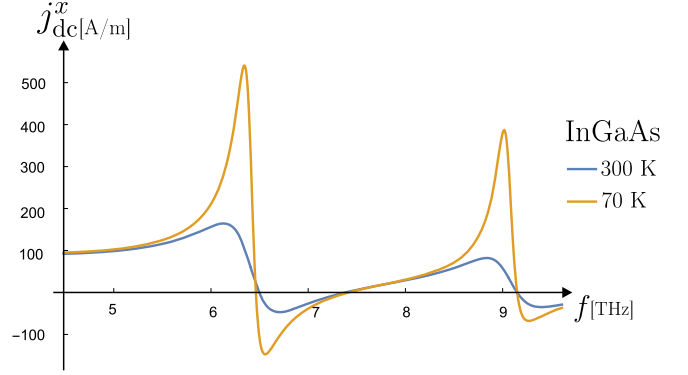


FIG. 8. Current-frequency dependence for parameters of InGaAs-based structure with  $d = 5a = 10R = 250$  nm at  $x = y = d/8$ , for two temperatures, 300 and 77 K.

Finally, we present a picture of the current for parameters of InGaAs-based structure with  $d = 5a = 10R = 250$  nm, for two temperatures, 300 and 77 K (see Fig. 8). We see resonance at the fundamental frequency  $f = f_0 = \omega_0/2\pi$  and the next one at the frequency  $\sqrt{2}f_0$ . As expected, the quality factor of plasmonic resonances increases with decreasing the temperature.

TABLE I. The estimated parameters for different structures

	Barrier thickness (nm)	T(k)	2D carrier density ( $1/\text{cm}^2$ )	$f=\omega_0/2\pi$ (THz)	$\gamma/\omega_0$	$e j_0$ (A/m)	$j_{dc}^m/j_0$	$e j_{dc}^m$ (A/m)	$H^m$ (Gs)
GaN	20	300	$10^{13}$	7	0.087	0.1	87	9	0.086
GaN	20	77	$10^{13}$	7	0.005	0.1	21897	2299	20.4
Si	4	300	$2 \cdot 10^{12}$	2.3	0.4	0.84	3.5	3	0.025
Si	4	77	$2 \cdot 10^{12}$	2.3	0.03	0.84	657	550	4.9
InGaAs	20	300	$2 \cdot 10^{12}$	6.4	0.089	0.89	84	74	0.64
InGaAs	20	77	$2 \cdot 10^{12}$	6.4	0.03	0.88	701	618	5.5
p-diamond	4	300	$2 \cdot 10^{12}$	1	0.08	0.8	112	89	0.78
p-diamond	4	77	$2 \cdot 10^{12}$	1	0.01	0.8	4815	3814	34

TABLE II. Material parameters used in the calculations

	Effective mass	Mobility $\text{cm}^2/\text{Vs}$ (77k)	Mobility $\text{cm}^2/\text{Vs}$ (300k)	Dielectric constant of material	Dielectric constant of barrier
Silicon	0.19[62]	20000[60]	1450[59]	11.9[62]	3.9
GaN	0.23[64]	31700[55]	2000[56]	8.9[62]	8.9
InGaAs	0.041[63]	35000[61]	12000[61]	13.9[62]	12.1
p-diamond	0.663[58]	35000[57]	5300[57]	5.7[62]	5.7

## VI. CONCLUSION

To conclude, we predicted excitation of circular plasmonic modes (twisted plasmons) in two dimensional elec-

tron liquid by circularly-polarized electromagnetic wave via a plasmonic coupler made of periodically placed

nanospheres. We demonstrated that rectification of the plasmons leads to a helicity-sensitive circular dc current, and consequently, to a magnetic moment, thus demonstrating the hydrodynamic inverse Faraday effect. This effect is dramatically increased in vicinity of plasmonic resonances, so that the dc current shows sharp plasmonic peaks. There are two interfering contributions to the peaks, the plasmonic contribution, and the contribution involving both the plasmonic and the Drude excitations. As a result, plasmonic resonances have asymmetric Fano-like shape. The suggested system can be used for optical tunable magnetization of 2D systems, for many optoelectronic devices operating in the THz range of frequencies, and for the characterization and parameter extraction of 2D electron liquids. In particular, measuring of the widths of different plasmonic resonances allows one to

extract the electron viscosity.

## VII. ACKNOWLEDGEMENT

The work of V.Yu.K. was supported by RFBR (Grant No. 20-02-00490), by Foundation for the Advancement of Theoretical Physics and Mathematics BASIS, and by the Foundation for Polish Science through the Grant No. MAB/2018/9 for CENTERA. The work at RPI was supported by the U.S. Army Research Laboratory Cooperative Research Agreement (Project Monitor Dr. Meredith Reed) and by the US ONR (Project Monitor Dr. Paul Maki).

### Appendix A: Linear response (technical details)

Linearizing Eqs. (2) and (3) and making Fourier transform we get

$$-i\omega\delta n_{\omega\mathbf{q}} + i\mathbf{q}\delta\mathbf{v}_{\omega\mathbf{q}} = 0, \quad (\text{A1})$$

$$i\mathbf{q}s^2\delta n_{\omega\mathbf{q}} + (\gamma - i\omega)\delta\mathbf{v}_{\omega\mathbf{q}} = \frac{e(\mathbf{E}_0 + \mathbf{E}_1)_{\omega\mathbf{q}}}{m}, \quad (\text{A2})$$

where

$$\left(\frac{e\mathbf{E}_0}{m}\right)_{\omega\mathbf{q}} = \frac{eE_0}{2m}(\mathbf{e}_x - i\mathbf{e}_y)(2\pi)^2\delta(\mathbf{q}) \quad (\text{A3})$$

$$\left(\frac{e\mathbf{E}_1}{m}\right)_{\omega\mathbf{q}} = -\frac{\pi\mathbf{q}e^2p}{m}e^{-i\varphi_{\mathbf{q}}}e^{-qa} \quad (\text{A4})$$

and  $e^{-i\varphi_{\mathbf{q}}} = (q_x - iq_y)/q$

Solution of Eqs. (A1), (A2) reads

$$\delta n_{\omega\mathbf{q}} = 2\pi il^2 \frac{q^2}{q^2 - k^2} e^{-i\varphi_{\mathbf{q}}} e^{-qa}, \quad (\text{A5})$$

$$\delta\mathbf{v}_{\omega\mathbf{q}} = 2\pi il^2 \frac{\omega\mathbf{q}}{q^2 - k^2} e^{-i\varphi_{\mathbf{q}}} e^{-qa} + \frac{eE_0(\mathbf{e}_x - i\mathbf{e}_y)}{2m(\gamma - i\omega)} (2\pi)^2\delta(\mathbf{q}), \quad (\text{A6})$$

where  $l$  and  $k$  are given by Eqs. (14) and (15) of the main text. Next, we find the Fourier transform of the velocity and concentration:

$$\delta n_{\omega}(\mathbf{r}) = \Delta Z(\mathbf{r}), \quad (\text{A7})$$

$$\delta\mathbf{v}_{\omega}(\mathbf{r}) = i\omega\nabla Z(\mathbf{r}) + \frac{eE_0(\mathbf{e}_x - i\mathbf{e}_y)}{2m(\gamma - i\omega)}, \quad (\text{A8})$$

where

$$\begin{aligned} Z(\mathbf{r}) &= -i2\pi l^2 \int \frac{d^2q}{(2\pi)^2} \frac{e^{i\mathbf{q}\mathbf{r}} e^{-i\varphi_{\mathbf{q}}} e^{-qa}}{q^2 - k^2} \\ &= l^2(x - iy)f(r). \end{aligned} \quad (\text{A9})$$

Function  $f(r)$  is given by

$$f(r) = \int_0^\infty \frac{dq q J_1(qr) e^{-qa}}{r(q^2 - k^2)} \approx \frac{\pi}{2r} [\mathbb{H}_{-1}(kr) + iJ_1(kr)] - \frac{1}{r} \left( 1 - \frac{r}{a + \sqrt{a^2 + r^2}} \right), \quad (\text{A10})$$

where  $\mathbb{H}_{-1}$  and  $J_1$  are the Struve and Bessel functions. Here we assumed  $Q \ll k_0 \ll 1/a$  [54].

The asymptotes of the function  $f$  are given by

$$f \approx \begin{cases} \sqrt{\frac{\pi}{2kr^3}} e^{i(kr - \pi/4)} \left( 1 + \frac{3i}{8kr} \right) - \frac{1}{k^2 r^3}, & r \gg 1/k_0, \\ \frac{1}{a + \sqrt{a^2 + r^2}} + \frac{i\pi k}{4}, & r \ll 1/k_0 \end{cases} \quad (\text{A11})$$

From Eqs. (24), (A7), and (A8) we get

$$\delta n_\omega^{\text{P}}(\mathbf{r}) = l^2(x - iy) \left[ f'' + \frac{3f'}{r} \right], \quad (\text{A12})$$

$$\delta \mathbf{v}_\omega^{\text{P}}(\mathbf{r}) = \omega l^2(x - iy) \left[ i \frac{(rf)'}{r} \mathbf{e}_r + \frac{f}{r} \mathbf{e}_\varphi \right], \quad (\text{A13})$$

$$\delta \mathbf{v}_\omega^{\text{D}}(\mathbf{r}) = \frac{eE_0(\mathbf{e}_x - i\mathbf{e}_y)}{2m(\gamma - i\omega)}. \quad (\text{A14})$$

As seen, the velocity oscillations can be presented as a sum of the  $f$ -dependent inhomogeneous contribution and the homogeneous Drude contribution, given, respectively, by Eq. (A13) and Eq. (A14)

### Appendix B: Expressions for $R_i^{\text{P}}$ and $\Phi_2^{\text{P}}$ for a single nanosphere

Using Eqs. (A10), (A11), (A12), (A13), (A14), and (18), we find

$$R_1^{\text{P}} = -i\omega l^4 (rf'' + 3f')(rf^*)' + c.c. \approx \pi\omega l^4 \begin{cases} \frac{k_0^2}{r} e^{-Qr}, & r > 1/k_0, \\ \frac{k_0 r}{2(r^2 + a^2)^{3/2}}, & r < 1/k_0, \end{cases} \quad (\text{B1})$$

$$\Phi_1^{\text{P}} = \omega l^4 (rf'' + 3f')f^* + c.c. \approx \pi\omega l^4 \begin{cases} -\frac{k_0}{r^2} e^{-Qr}, & r > 1/k_0, \\ -\frac{2}{\pi} \frac{r}{(r^2 + a^2)^{3/2}(a + \sqrt{r^2 + a^2})}, & r < 1/k_0, \end{cases} \quad (\text{B2})$$

$$R_2^{\text{P}} = -\frac{\omega^2 l^4}{\gamma} [(rf^*)'(rf)'' + f^* f'] + c.c. \approx \frac{\pi\omega^2 l^4}{\gamma} \begin{cases} \frac{k_0}{2r^2} (1 + Qr) e^{-Qr}, & r > 1/k_0, \\ \frac{2}{\pi} \frac{r}{(a + \sqrt{r^2 + a^2})^3} \left[ \frac{a^3}{(a^2 + r^2)^2} + \frac{r^2 + 3a^2}{(a^2 + r^2)^{3/2}} \right], & r < 1/k_0, \end{cases} \quad (\text{B3})$$

$$\Phi_2^{\text{P}} = 0. \quad (\text{B4})$$

### Appendix C: Expressions for $R_i^{\text{M}}$ and $\Phi_i^{\text{M}}$ for a single nanosphere

By direct averaging of  $\delta n^{\text{P}} \delta \mathbf{v}^{\text{D}}$  over time we get

$$R_1^{\text{M}} - i\Phi_1^{\text{M}} = \frac{2l^4 s^2 r f'' + 3f'}{R^3 \gamma + i\omega}. \quad (\text{C1})$$

In the limiting cases, assuming  $\omega \gg \gamma$  and taking in all terms lowest non-zero order with respect to  $\gamma/\omega$  we get

$$R_1^M = \frac{2l^4 s^2}{R^3} \begin{cases} \frac{\sqrt{\pi} k_0^{3/2} e^{-Qr/2} \cos(k_0 r + \frac{\pi}{4})}{\omega \sqrt{2r}}, & r > 1/k_0 \\ -\frac{\gamma}{\omega^2} \frac{r}{(r^2 + a^2)^{3/2}}, & r < 1/k_0 \end{cases} \quad (C2)$$

and

$$\Phi_1^M = -\frac{2l^4 s^2}{\omega R^3} \begin{cases} \frac{\sqrt{\pi} k_0^{3/2} e^{-Qr/2} \sin(k_0 r + \frac{\pi}{4})}{\sqrt{2r}}, & r > 1/k_0 \\ \frac{r}{(r^2 + a^2)^{3/2}}, & r < 1/k_0 \end{cases} \quad (C3)$$

Finally, from Eqs. (18), (A13), and (A14) we find (in the lowest order with respect to  $\gamma/\omega$ )

$$R_2^M = -\frac{l^4 s^2}{\gamma R^3} (r f'' + 3f') + c.c. \\ = \frac{2l^4 s^2}{\gamma R^3} \begin{cases} \frac{\sqrt{\pi} k_0^{3/2} e^{-Qr/2} \sin(k_0 r + \frac{\pi}{4})}{\sqrt{2r}}, & r > 1/k_0, \\ \frac{r}{(a^2 + r^2)^{3/2}}, & r < 1/k_0, \end{cases} \quad (C4)$$

$$\Phi_2^M = 0. \quad (C5)$$

#### Appendix D: Asymptotical values of $j_{dc}$ and $E_{dc}$ for a single nanosphere

Using Eqs. (B1),(B2),(B3),(B4), (C2),(C3),(C4), and (C5), we find asymptotical behavior of  $j_{dc}$  and  $E_{dc}$  with account of both plasmonic and mixed contribution

$$j^{dc} = -\frac{\omega l^4 N_0}{a^3} \begin{cases} A\left(\frac{r}{a}\right) + \frac{a}{R^3 k_0^2} C\left(\frac{r}{a}\right), & r \ll 1/k_0, \\ \frac{\pi a^3}{r^3} \left[ k_0 r e^{-Qr} + \sqrt{\frac{2}{\pi k_0 r}} \left(\frac{r}{R}\right)^3 e^{-Qr/2} \sin\left(k_0 r + \frac{\pi}{4}\right) \right], & 1/k_0 \ll r \ll \frac{\ln[k_0/Q]}{Q} \\ 6a^3 \left( -\frac{1}{k_0^7 r^7} + \frac{1}{R^3 k_0^4 r^4} \right), & \frac{\ln[k_0/Q]}{Q} \ll r, \end{cases} \quad (D1)$$

$$\frac{eE^{dc}}{m} = -\frac{\omega^2 l^4}{a^3} \begin{cases} \pi B\left(\frac{r}{a}\right) + \frac{a}{R^3 k_0^2} C\left(\frac{r}{a}\right), & r \ll 1/k_0, \\ \frac{\pi a^3}{r^3} \left[ \frac{k_0 r}{2} e^{-Qr} + \sqrt{\frac{2}{\pi k_0 r}} \left(\frac{r}{R}\right)^3 e^{-Qr/2} \sin\left(k_0 r + \frac{\pi}{4}\right) \right], & 1/k_0 \ll r \ll \frac{\ln[k_0/Q]}{Q}, \\ 6a^3 \left( \frac{5}{k_0^7 r^7} + \frac{1}{R^3 k_0^4 r^4} \right), & \frac{\ln[k_0/Q]}{Q} \ll r, \end{cases} \quad (D2)$$

where

$$A(x) = \frac{2x}{(1+x^2)^{3/2}(1+\sqrt{1+x^2})}, \quad (D3)$$

$$B(x) = \frac{2x}{(1+\sqrt{1+x^2})^3} \frac{1+(3+x^2)\sqrt{1+x^2}}{(1+x^2)^2},$$

$$C(x) = \frac{2x}{(1+x^2)^{3/2}} \quad (D4)$$

**Appendix E: Expressions for  $\mathbf{J}_i^P, \mathbf{J}_i^M$  for periodic array of nanospheres.**

For a periodic array of nanospheres one should replace  $Z(\mathbf{r})$  with the following sum

$$\sum_{n,m} Z(\mathbf{r} - \mathbf{r}_{nm}) = \sum_{n,m} \int \frac{d^2\mathbf{q}}{(2\pi)^2} Z_{\mathbf{q}} e^{-i\mathbf{q}\mathbf{r}_{nm}} e^{i\mathbf{q}\mathbf{r}}, \quad (\text{E1})$$

where  $Z(\mathbf{r})$  is given by Eq. (13) and

$$\mathbf{r}_{nm} = d(n\mathbf{e}_x + m\mathbf{e}_y) \quad (\text{E2})$$

are lattice vectors of the squared array. Next, we use the Poisson summation formula

$$\sum_{n,m} e^{-i\mathbf{q}\mathbf{r}_{nm}} = \sum_n e^{-idq_x n} \sum_m e^{-idq_y m} = \left(\frac{2\pi}{d}\right)^2 \sum_m \delta\left(q_x - \frac{2\pi m}{d}\right) \sum_n \delta\left(q_y - \frac{2\pi n}{d}\right). \quad (\text{E3})$$

Substituting Eq. (E3) into Eq. (E1) and integrating over  $d^2\mathbf{q}$  we get

$$\sum_{n,m} Z(\mathbf{r} - \mathbf{r}_{nm}) = \frac{1}{d^2} \sum_{\mathbf{q}=\mathbf{q}_{nm}} Z_{\mathbf{q}} e^{i\mathbf{q}\mathbf{r}}, \quad (\text{E4})$$

where inverse lattice vectors  $\mathbf{q}_{nm}$  are given by Eq. (17).

The rectified currents  $\mathbf{J}_i^P$  are given by double sums over  $\mathbf{q}, \mathbf{q}'$  (both  $\mathbf{q}$  and  $\mathbf{q}'$  run over values  $\mathbf{q}_{nm}$ ), while  $\mathbf{J}_i^M$  by ordinary ones. For convenience of further calculations, in plasmonic contribution we introduce Kronecker symbol  $\delta_{\mathbf{Q}, \mathbf{q}-\mathbf{q}'}$  and sum over  $\mathbf{Q}$ :

$$\mathbf{J}_1^P(\mathbf{r}) = \sum_{\mathbf{Q}} e^{i\mathbf{Q}\mathbf{r}} \mathbf{J}_{1\mathbf{Q}}^P + c.c. = \frac{4\pi^2 l^4}{d^4} \sum_{\mathbf{Q}} e^{i\mathbf{Q}\mathbf{r}} \sum_{\mathbf{q}, \mathbf{q}'} \delta_{\mathbf{Q}, \mathbf{q}-\mathbf{q}'} \frac{e^{-i(\varphi_{\mathbf{q}} - \varphi_{\mathbf{q}'}) - a(q+q')} \omega \mathbf{q} \mathbf{q}'^2}{(q^2 - k^2)(q'^2 - k^{*2})} + c.c. \quad (\text{E5})$$

$$\mathbf{J}_2^P(\mathbf{r}) = \sum_{\mathbf{Q}} e^{i\mathbf{Q}\mathbf{r}} \mathbf{J}_{2\mathbf{Q}}^P + c.c. = \frac{4i\pi^2 l^4}{d^4 \gamma} \sum_{\mathbf{Q}} e^{i\mathbf{Q}\mathbf{r}} \sum_{\mathbf{q}, \mathbf{q}'} \delta_{\mathbf{Q}, \mathbf{q}-\mathbf{q}'} \frac{e^{-i(\varphi_{\mathbf{q}} - \varphi_{\mathbf{q}'}) - a(q+q')} \omega^2 (\mathbf{q}\mathbf{q}') \mathbf{q}'}{(q^2 - k^2)(q'^2 - k^{*2})} + c.c. \quad (\text{E6})$$

$$\mathbf{J}_1^M(\mathbf{r}) = \sum_{\mathbf{Q}} e^{i\mathbf{Q}\mathbf{r}} \mathbf{J}_{1\mathbf{Q}}^M + c.c. = \frac{2i\pi l^4 s^2}{d^2 R^3} \frac{1}{\gamma + i\omega} \sum_{\mathbf{Q}} \frac{e^{i\mathbf{Q}\mathbf{r} - i\varphi_{\mathbf{Q}} - aQ} Q^2}{(Q^2 - k^2)} (\mathbf{e}_x + i\mathbf{e}_y) + c.c. \quad (\text{E7})$$

$$\mathbf{J}_2^M(\mathbf{r}) = \sum_{\mathbf{Q}} e^{i\mathbf{Q}\mathbf{r}} \mathbf{J}_{2\mathbf{Q}}^M + c.c. = \frac{2\pi l^4 s^2}{d^2 R^3 \gamma} \frac{1}{\gamma + i\omega} \sum_{\mathbf{Q}} \frac{e^{i\mathbf{Q}\mathbf{r}} e^{-aQ} \omega \mathbf{Q} \mathbf{Q}}{Q^2 - k^2} + h.c. \quad (\text{E8})$$

Using Eqs. (31) and (32) we find expression for optically-induced dc current, which includes both plasmonic and mixed contributions:

$$\mathbf{j}^{dc} = N_0 \frac{4\pi^2 l^4}{d^4} \left\{ \omega \sum_{\mathbf{q}, \mathbf{q}'} \frac{[\mathbf{e}_z \times (\mathbf{q} - \mathbf{q}')] \left( \frac{[\mathbf{e}_z \times (\mathbf{q} - \mathbf{q}')] \mathbf{q}}{|\mathbf{q} - \mathbf{q}'|} \right)}{|\mathbf{q} - \mathbf{q}'|} \frac{q'^2 e^{i(\mathbf{q}-\mathbf{q}')\mathbf{r}} e^{-i(\varphi_{\mathbf{q}} - \varphi_{\mathbf{q}'}) - a(q+q')}}{(q^2 - k^2)(q'^2 - k^{*2})} \right. \\ \left. + \frac{is^2 d^2}{2\pi R^3} \frac{1}{\gamma + i\omega} \sum_{\mathbf{Q}} \frac{[\mathbf{e}_z \times \mathbf{Q}]}{Q} \left( \frac{[\mathbf{e}_z \times \mathbf{Q}] (\mathbf{e}_x + i\mathbf{e}_y)}{Q} \right) \frac{Q^2 e^{i\mathbf{Q}\mathbf{r} - i\varphi_{\mathbf{Q}} - aQ}}{Q^2 - k^2} \right\} + c.c. \quad (\text{E9})$$

$$\frac{e\mathbf{E}_{dc}}{m} = \gamma \sum_{\mathbf{Q}} \frac{\mathbf{Q}}{Q} \left\{ \frac{\mathbf{Q}}{Q} [\mathbf{J}_{1\mathbf{Q}}^P + \mathbf{J}_{2\mathbf{Q}}^P + \mathbf{J}_{1\mathbf{Q}}^M + \mathbf{J}_{2\mathbf{Q}}^M] \right\} e^{i\mathbf{Q}\mathbf{r}} + c.c. \quad (\text{E10})$$

$$\approx (\text{for } \gamma \ll \omega) \approx \gamma \sum_{\mathbf{Q}} \frac{\mathbf{Q}}{Q} \left\{ \frac{\mathbf{Q}}{Q} [\mathbf{J}_{2\mathbf{Q}}^P + \mathbf{J}_{2\mathbf{Q}}^M] \right\} e^{i\mathbf{Q}\mathbf{r}} + c.c. \quad (\text{E11})$$

$$= \frac{4\pi^2 l^4}{d^4} \left\{ i\omega^2 \sum_{\mathbf{q}, \mathbf{q}'} \frac{\mathbf{q} - \mathbf{q}'}{|\mathbf{q} - \mathbf{q}'|} \left[ \frac{(\mathbf{q} - \mathbf{q}') \mathbf{q}'}{|\mathbf{q} - \mathbf{q}'|} \right] \frac{(\mathbf{q}\mathbf{q}') e^{i(\mathbf{q}-\mathbf{q}')\mathbf{r}} e^{-i(\varphi_{\mathbf{q}} - \varphi_{\mathbf{q}'}) - a(q+q')}}{(q^2 - k^2)(q'^2 - k^{*2})} \right. \\ \left. - i \frac{s^2 d^2}{2\pi R^3} \sum_{\mathbf{Q}} \frac{Q \mathbf{Q} e^{i\mathbf{Q}\mathbf{r} - aQ}}{Q^2 - k^2} \right\} + c.c. \quad (\text{E12})$$

### Appendix F: Expressions for rectified currents in the fundamental plasmonic mode

For  $(n, m) = (1, 0), (0, 1), (-1, 0), (0, -1)$ , we have  $q = q_0 = 2\pi/d$ . Simple calculations yield

$$\mathbf{J}_1^{\text{P}} = \frac{32\pi^2 l^4}{d^4} \frac{\omega q_0^3 [\sin(q_0 y) \cos(q_0 x) \mathbf{e}_x - \sin(q_0 x) \cos(q_0 y) \mathbf{e}_y]}{|q_0^2 - k^2|^2} e^{-2q_0 a}, \quad (\text{F1})$$

$$\mathbf{J}_2^{\text{P}} = \frac{32\pi^2 l^4}{d^4} \frac{\omega^2 q_0^3 [\sin(q_0 x) \cos(q_0 x) \mathbf{e}_x + \sin(q_0 y) \cos(q_0 y) \mathbf{e}_y]}{\gamma |q_0^2 - k^2|^2} e^{-2q_0 a}, \quad (\text{F2})$$

$$\mathbf{J}_1^{\text{M}} = \frac{4\pi l^4}{d^2 R^3} \frac{q_0^2 \omega}{k_*^2 (q_0^2 - k^2)} [i \sin(q_0 x) + \sin(q_0 y)] (\mathbf{e}_x + i \mathbf{e}_y) e^{-q_0 a} + c.c. \quad (\text{F3})$$

$$\mathbf{J}_2^{\text{M}} = \frac{4\pi l^4}{d^2 R^3} \frac{q_0^2 \omega^2}{\gamma k_*^2 (q_0^2 - k^2)} [\sin(q_0 x) \mathbf{e}_x + \sin(q_0 y) \mathbf{e}_y] e^{-q_0 a} + c.c. \quad (\text{F4})$$

Next, we substitute these equations into Eqs. (32) and (33). The latter can be written in the operator form

$$\mathbf{j}_{\text{dc}} = N_0 \frac{-\nabla \text{div} + \Delta}{\Delta} (\mathbf{J}_1^{\text{P}} + \mathbf{J}_1^{\text{M}}), \quad (\text{F5})$$

$$\frac{e \mathbf{E}_{\text{dc}}}{m} = \gamma \frac{\nabla}{\Delta} \text{div} (\mathbf{J}_1^{\text{P}} + \mathbf{J}_1^{\text{M}} + \mathbf{J}_2^{\text{P}} + \mathbf{J}_2^{\text{M}}), \quad (\text{F6})$$

$$\frac{e \phi_{\text{dc}}}{m} = \gamma \frac{1}{\Delta} \text{div} (\mathbf{J}_1^{\text{P}} + \mathbf{J}_1^{\text{M}} + \mathbf{J}_2^{\text{P}} + \mathbf{J}_2^{\text{M}}). \quad (\text{F7})$$

From Eqs. (F1), (F2), (F3), (F4), (F5), (F6), and (F7), we find

$$\begin{aligned} \mathbf{j}_{\text{dc}} = N_0 & \left\{ \frac{16\pi^2 l^4}{d^4} \frac{\omega q_0^3 e^{-2q_0 a} [\sin(q_0 y) \cos(q_0 x) \mathbf{e}_x - \sin(q_0 x) \cos(q_0 y) \mathbf{e}_y]}{|q_0^2 - k^2|^2} \right. \\ & \left. + \frac{4\pi l^4}{d^2 R^3} \frac{\omega q_0^2 e^{-q_0 a} [\sin(q_0 y) \mathbf{e}_x - \sin(q_0 x) \mathbf{e}_y]}{k_*^2 (q_0^2 - k^2)} \right\} + c.c. \end{aligned} \quad (\text{F8})$$

Close to resonance, this equation can be simplified and written in the form of Eq. (22) with  $\boldsymbol{\pi}$  and  $\boldsymbol{\mu}$  given by Eq. (40) and (41), respectively. We also find (for  $\gamma \ll \omega$ )

$$\begin{aligned} \frac{e \mathbf{E}_{\text{dc}}}{m} = & \left\{ \frac{16\pi^2 l^4}{d^4} \frac{\omega^2 q_0^3 e^{-2q_0 a} [\sin(q_0 x) \cos(q_0 x) \mathbf{e}_x + \sin(q_0 y) \cos(q_0 y) \mathbf{e}_y]}{|q_0^2 - k^2|^2} \right. \\ & \left. + \frac{4\pi l^4}{d^2 R^3} \frac{\omega^2 q_0^2 e^{-q_0 a} [\sin(q_0 x) \mathbf{e}_x + \sin(q_0 y) \mathbf{e}_y]}{k_*^2 (q_0^2 - k^2)} \right\} + c.c., \end{aligned} \quad (\text{F9})$$

$$\begin{aligned} \frac{e \phi_{\text{dc}}}{m} = & \left\{ \frac{4\pi^2 l^4}{d^4} \frac{\omega^2 q_0^2 e^{-2q_0 a} [\cos(2q_0 x) + \cos(2q_0 y)]}{|q_0^2 - k^2|^2} \right. \\ & \left. + \frac{4\pi l^4}{d^2 R^3} \frac{\omega^2 q_0 e^{-q_0 a} [\cos(q_0 x) + \cos(q_0 y)]}{k_*^2 (q_0^2 - k^2)} \right\} + c.c. \end{aligned} \quad (\text{F10})$$

- 
- [1] L. P. Pitaevskii, Sov. Phys. JETP 12, 1008 (1961)[J. Exp. Theor. Phys. **39**, 1450 (1960)]  
[2] J. P. van der Ziel, P. S. Pershan and L. D. Malmstrom, Phys. Rev. Lett. **15**, 190 (1965).  
[3] A. V. Kimel, A. Kirilyuk, P. A. Usachev, R. V. Pisarev, A. M. Balbashov and Th. Rasing, Nature **435**, 655 (2005).

- [4] A. Kirilyuk, A. V. Kimel, and T. Rasing, Rev. Mod. Phys. **82**, 2731 (2010).  
[5] A. Kirilyuk, A. V. Kimel and Th. Rasing, Phil. Trans. R. Soc. A **369**, 3631 (2011).  
[6] O. V. Kibis, Phys. Rev. Lett. **107**, 106802 (2011).  
[7] O. V. Kibis, O. Kyriienko, I. A. Shelykh, Phys. Rev. B **87**, 245437 (2013).



- [8] A. M. Alexeev, I. A. Shelykh, M. E. Portnoi, Phys. Rev. B **88**, 085429 (2013).
- [9] F. K. Joibari, Ya. M. Blanter, G. E. W. Bauer, Phys. Rev. B **90**, 155301 (2014).
- [10] A. M. Alexeev, M. E. Portnoi, Phys. Rev. B **85**, 245419 (2012).
- [11] V. V. Kruglyak, M. E. Portnoi, Technical Physics Letters, **31**, 1047 (2005) [Pisma v Zh. Tekh. Fiziki **31**, 20 (2005)].
- [12] V. V. Kruglyak, M. E. Portnoi, R. J. Hicken, Journal of Nanophotonics, **1**, 013502 (2007).
- [13] M. L. Polianski, Phys. Rev. B **80**, 241301(R) (2009).
- [14] K. L. Koshelev, V. Yu. Kachorovskii, and M. Titov, Phys. Rev. B **92**, 235426 (2015).
- [15] K. L. Koshelev, V. Yu. Kachorovskii, M. Titov, and M. S. Shur, Phys. Rev. B **95**, 035418 (2017).
- [16] M. I. Dyakonov and M. S. Shur, Phys. Rev. Lett. **71**, 2465 (1993).
- [17] E. L. Ivchenko and S. D. Ganichev, Pisma v ZheTF **93**, 752 (2011) [JETP Lett. **93**, 673 (2011)].
- [18] J. B. Khurgin, Nature Nanotechnology **10**, 2 (2015).
- [19] P. Nordlander, Nature Nanotechnology **8**, 76 (2013).
- [20] J. Heber, Nature Materials **11**, 745 (2012).
- [21] A. N. Grigorenko, M. Polini, K. S. Novoselov, Nature Photonics **6**, 749 (2012).
- [22] F. H. L. Koppens, D. E. Chang, F. J. Garcia de Abajo, Nano Lett. **11**, 3370 (2011).
- [23] D. K. Gramotnev and S. I. Bozhevolnyi, Nature Photonics **4**, 83 (2010).
- [24] S. A. Maier, *Plasmonics: Fundamentals and Applications* (Springer, NY, USA, 2007).
- [25] R. N. Gurzhi, Usp. Fiz. Nauk **94**, 689 (1968) [Sov. Phys. Usp. **11**, 255 (1968)].
- [26] M. J. M. de Jong, L. W. Molenkamp, Phys. Rev. B **51**, 13389 (1995).
- [27] M. I. Dyakonov and M. S. Shur, Phys. Rev. B **51**, 14341 (1995).
- [28] M. I. Dyakonov and M. S. Shur, IEEE Trans. on Elec. Dev. **43**, 380 (1996).
- [29] A. P. Dmitriev, A. S. Furman, and V. Yu. Kachorovskii, Phys. Rev. B **54**, 14020 (1996).
- [30] A. P. Dmitriev, A. S. Furman, V. Yu. Kachorovskii, G. G. Samsonidze, and Ge. G. Samsonidze, Phys. Rev. B **55**, 10319 (1997).
- [31] T. Otsuji and M. S. Shur, IEEE Microwave Magazine, **15**, 43 (2014).
- [32] W. Knap, D. B. But, N. Dyakonova, D. Coquillat, A. Gutin, O. Klimenko, S. Blin, F. Teppe, M. S. Shur, T. Nagatsuma, S. D. Ganichev, and T. Otsuji, *Recent Results on Broadband Nanotransistor Based THz Detectors* in NATO Science for Peace and Security Series B, Physics and Biophysics: THz and Security Applications, edited by C. Corsi, F. Sizov, (Springer, Dordrecht, Netherlands, 2014).
- [33] R. Jaggi, J. Appl. Phys. **69**, 816 (1991).
- [34] R. N. Gurzhi, A. N. Kalinenko, and A. I. Kopeliovich, Phys. Rev. Lett. **74**, 3872 (1995).
- [35] K. Damle, S. Sachdev, Phys. Rev. B **56**, 8714 (1997).
- [36] H. Buhmann, L. W. Molenkamp, R. N. Gurzhi, A. N. Kalinenko, A. I. Kopeliovich and A. V. Yanovsky, Low Temp. Phys. **24**, 737 (1998).
- [37] H. Predel, H. Buhmann, L. W. Molenkamp, R. N. Gurzhi, A. N. Kalinenko, A. I. Kopeliovich, and A. V. Yanovsky, Phys. Rev. B **62**, 2057 (2000).
- [38] A. V. Andreev, S. A. Kivelson, and B. Spivak, Phys. Rev. Lett. **106**, 256804 (2011).
- [39] D. Forcella, J. Zaanen, D. Valentinis, and D. van der Marel, Phys. Rev. B **90**, 035143 (2014).
- [40] A. Tomadin, G. Vignale, and M. Polini, Phys. Rev. Lett. **113**, 235901 (2014).
- [41] P. S. Alekseev, Phys. Rev. Lett. **117**, 166601 (2016)
- [42] A. B. Kashuba, Phys. Rev. B **78**, 085415 (2008).
- [43] L. Fritz, J. Schmalian, M. Müller, and S. Sachdev, Phys. Rev. B **78**, 085416 (2008).
- [44] M. Müller, J. Schmalian, and L. Fritz, Phys. Rev. Lett. **103**, 025301 (2009).
- [45] M. Mendoza, H. J. Herrmann, and S. Succi, Phys. Rev. Lett. **106**, 156601 (2011).
- [46] B. N. Narozhny, I. V. Gornyi, M. Titov, M. Schütt, and A. D. Mirlin, Phys. Rev. B **91**, 035414 (2015).
- [47] A. Cortijo, Y. Ferreirós, K. Landsteiner, and M. A. H. Vozmediano, Phys. Rev. Lett. **115**, 177202 (2015).
- [48] L. Levitov, G. Falkovich, Nat. Phys. **12**, 672 (2016).
- [49] G. Falkovich and L. Levitov, Phys. Rev. Lett. **119**, 066601 (2017).
- [50] Sven Danz and Boris N Narozhny, 2D Materials **7**, 3 (2020).
- [51] H.-Y. Xie and A. Levchenko, Phys. Rev. B **99**, 045434 (2019).
- [52] S. Danz, M. Titov, B. N. Narozhny (2019), arXiv:1912.12341
- [53] We assume for simplicity that embedding matrix and substrate have the same dielectric constant  $\epsilon$ .
- [54] This equation interpolates between asymptotes at  $r \gg a$ , where one can put  $a = 0$  and the case  $r \ll 1/|k|$ , where one can use expansion over  $k$  up to the first order with the parametrical matching at  $a \ll r \ll 1/|k|$ .
- [55] E. Borovitskaya, W. Knap, M. S. Shur, R. Gaska, E. Frayssinet, P. Lorenzini, N. Grandjean, B. Baumont, J. Massies, C. Skierbiszewski, P. Prystawko, M. Leszczynski, I. Grzegory, and S. Porowski, (2000). Two-dimensional electron gas scattering mechanisms in AlGaIn/GaN heterostructures. MRS Proceedings, 639. (2020)
- [56] R. Gaska, M. S. Shur, A. D. Bykhovskii, A. O. Orlov, and G. L. Snider, Appl. Phys. Lett. **74**, 287 (1999)
- [57] I. Akimoto, Y. Handa, K. Fukai, and N. Naka, Appl. Phys. Lett. **105**, 032102 (2014)
- [58] N. Naka, K. Fukai, Y. Handa, and I. Akimoto, Phys. Rev. B **88**, 035205 (2013)
- [59] Pietro P. Altermatt, Andreas Schenk, Frank Geelhaar Gernot Heiser, J. of Appl. Phys. **93**, 1598 (2003)
- [60] <http://www.semiconductors.co.uk/propiviv5431.htm>
- [61] Goldberg Yu. A. and N. M. Schmidt "Handbook Series on Semiconductor Parameters", **2**, M. Levinstein, S. Rumyantsev and M. Shur, ed., World Scientific, London, pp. 62-88 (1999).
- [62] M. E. Levinstein, S. Rumyantsev, and M. S. Shur, Editors, "Handbook of Semiconductor Material Parameters, Si, Ge, C (diamond), GaAs, GaP, GaSb, InAs, InP, InSb" **1**, World Scientific, ISBN981-02-2934-8517, Singapore (1996).
- [63] R. J. Nicholas, J. C. Portal, C. Houlbert, P. Perrier and T. P. Pearsall, Appl. Phys. Lett **34**, 492 (1979)
- [64] W. Knap, V. I. Falko, E. Frayssinet, P. Lorenzini, N. Grandjean, D. Maude, G. Karczewski, B. L. Brandt, J. Lusakowski, I. Grzegory, M. Leszczynski, P. Prystawko, C. Skierbiszewski, S. Porowski, X. Hu, G. Simin, M. A.

Khan, and M. S. Shur, *J. Phys. Condens. Matter* **16** 1  
(2004)